Twisted-torus configurations with large toroidal magnetic fields in relativistic stars

R. Ciolfi and L. Rezzolla

Max-Planck-Institut für Gravitationsphysik, Albert-Einstein-Institut, Potsdam, Germany

7 May 2014

ABSTRACT

Understanding the properties of the internal magnetic field of neutron stars remains a theoretical challenge. Over the last years, twisted-torus geometries have been considered both in Newtonian and general-relativistic equilibrium models, as they represent a potentially good description of neutron star interiors. All of these works have found an apparent intrinsic limitation to geometries that are *poloidal-field-dominated*, with a toroidal-to-poloidal energy ratio inside the star that are $\lesssim 10\%$, unless surface currents are included and magnetic fields are allowed to be discontinuous. This limitation is in stark contrast with the general expectation that much higher toroidal fields should be present in the stellar interior and casts doubt about the stability and hence realism of these configurations. We here discuss how to overcome this limitation by adopting a new prescription for the azimuthal currents that leads to magnetized equilibria where the toroidal-to-total magnetic-field energy ratio can be as high as 90%, thus including geometries that are *toroidal-field-dominated*. Moreover, our results show that for a fixed exterior magnetic-field strength, a higher toroidal-field energy implies a much higher total magnetic energy stored in the star, with a potentially strong impact on the expected electromagnetic and gravitational-wave emission from highly magnetized neutron stars.

Key words: stars: neutron — gravitational waves — magnetohydrodynamics (MHD) — methods: numerical

1 INTRODUCTION

Magnetic fields represent a key aspect of the physics and astrophysics of neutron stars (NSs). Observational evidence points at very strong external (polar) magnetic field strengths, up to 10^{13} G for ordinary NSs and 10^{15} G for magnetars (Duncan & Thompson 1992), while the internal fields might be even stronger. All the dynamical processes connected to present observations of NSs are affected or even directly produced by magnetic fields as, for example, the dipole radiation or the magnetar flaring activity. Moreover, magnetically induced deformations of the stellar structure can make rotating neutron stars potentially detectable sources of gravitational waves (GWs) (Bonazzola & Gourgoulhon 1996; Cutler 2002; Frieben & Rezzolla 2012). Both the GW and the electromagnetic emissions depend sensitively on the amount of magnetic field energy stored in the NS and on its geometrical distribution. Despite its great relevance, observations have not yet provided direct constraints on the internal magnetic-field configuration.

Understanding the properties of the internal magnetic field of NSs is a theoretical challenge which dates back to the early work of Chandrasekhar & Fermi (1953). Since then, a number or analytical and numerical studies have been devoted to the construction of equilibrium models of magnetized NSs, at first considering the simple purely poloidal and purely toroidal geometries. However, already from the analytical work on nonrotating magnetized stars

of Markey & Tayler (1973), Wright (1973) and Tayler (1973), there has been growing evidence that these simple geometries would suffer from the so-called Tayler (or kink) instability, acting on Alfvén timescales, and that a long-lived magnetic field has to consist of mixed poloidal-toroidal fields. These perturbative predictions have recently seen a number of confirmations through fully nonlinear simulations in general relativity (Lasky et al. 2011; Ciolfi et al. 2011; Ciolfi & Rezzolla 2012; Kiuchi et al. 2011). These studies also show that a significant magnetic helicity is produced and that the system tends to an equipartion between poloidal and toroidal fields (Ciolfi & Rezzolla 2012). Unfortunately, the prospects of detecting GWs produced by the instability are pessimistic (Zink et al. 2012; Lasky et al. 2012; Ciolfi & Rezzolla 2012).

Among the possible configurations with a mixed magnetic field, the so-called *twisted-torus* geometry has recently emerged as a good candidate for NS interiors. It consists of an axisymmetric mixed field where the poloidal component extends throughout the entire star and to the exterior, while the toroidal one is confined inside the star, in the torus-shaped region where the poloidal field lines are closed. An important feature of this geometry is that the magnetic field is not entirely confined to the interior of the star, as considered, e.g., by Ioka & Sasaki (2004), Haskell et al. (2008), Duez & Mathis (2010) and Yoshida et al. (2012), thus in better agreement with the observational evidence of external fields. Furthermore, in a twisted-torus configuration both of the magnetic-

field components are continuous at the stellar surface. A discontinuity in the magnetic field would require the inclusion of surface currents (Colaiuda et al. 2008), for which there is no obvious way to generate and sustain them. An important indication in favour of the twisted-torus configuration comes from the work of Braithwaite & Nordlund (2006), where this geometry emerged as the final outcome of the evolution of initial random fields in a nonrotating fluid star. A twisted-torus magnetic field also appears natural in terms of the poloidal and toroidal-field instabilities. The first one takes place in the closed-line region and produces there a stabilizing toroidal component, while the toroidal-field instability occurs near the symmetry axis and produces there a poloidal field.

Over the last years, twisted-torus geometries were considered in Newtonian (Tomimura & Eriguchi 2005; Yoshida & Eriguchi 2006; Lander & Jones 2009, 2012; Glampedakis et al. 2012; Fujisawa et al. 2012) and general-relativistic frameworks (Ciolfi et al. 2009, 2010; hereafter Paper I and Paper II). In spite the different approaches adopted, all the twisted-torus models proposed so far have given rather similar results in terms of the possible configuration of magnetic fields. The most important of these results is the apparently unavoidable restriction to *poloidal-field-dominated* geometries, with an upper limit of ∼ 10% for the toroidal-to-poloidal energy ratio in the star, unless surface currents and discontinuous magnetic fields are included (Fujisawa & Eriguchi 2013).

This limitation is far more serious than it may appear. First, a much higher toroidal-field content is expected from the formation scenario of highly magnetized NSs, simply as a result of strong differential rotation in the nascent NS (Thompson & Duncan 1993; Bonanno et al. 2003). Second, higher toroidal-field energies are needed when considering the magneto-thermal evolution of magnetars, their bursting activity and the pulse profiles (Pons & Perna 2011). Finally, all evidence is that poloidal-field-dominated geometries are unstable on Alfvén timescales (Braithwaite 2009; Lander & Jones 2012; Lasky et al. 2011; Ciolfi et al. 2011) and hence the twisted-torus configurations considered so far may not be realistic.

In this Letter we overcome this limitation by adopting a new prescription for the azimuthal currents that leads to more generic twisted-torus configurations. In this way we construct a new sample of magnetized equilibria where the toroidal-to-total magnetic-field energy ratio can be as high as 90%, thus including *toroidal-field-dominated* geometries. Moreover, we find that for a fixed exterior magnetic field strength, a higher relative content of toroidal field energy implies a much higher total magnetic energy in the star, with a potentially strong impact on the expected electromagnetic and GW emission properties of highly magnetized NSs.

2   THE MATHEMATICAL MODEL

We consider axisymmetric equilibrium configurations of a non-rotating magnetized NS, infinitely conducting and surrounded by vacuum, obtained assuming that the magnetic field acts as a perturbation of a spherically symmetric background star [see Paper I for a discussion on these assumptions and on the conditions under which a superfluid interior may not be considered (Lander 2013)]. The background NS has a (gravitational) mass of $M = 1.4 \, M_\odot$ and is described as a barotropic fluid with polytropic equation of state (EOS) $p = K\rho^\Gamma$, where p is the fluid pressure and ρ the rest-mass density, with $K = 100$ and $\Gamma = 2$ (in units in which $c = G = M_\odot = 1$). More sophisticated EOSs could be considered
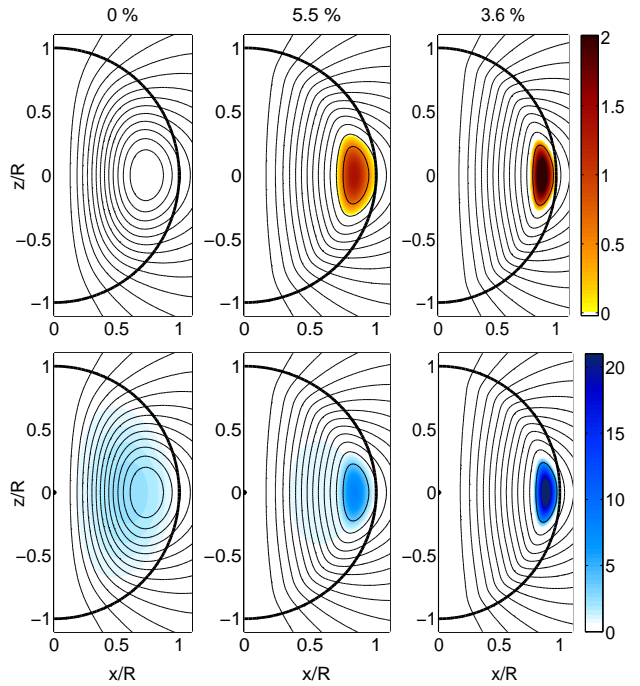

Figure 1. *Top panels:* Meridional view of magnetic field configurations obtained with constant $F(\psi)$. Shown in colour is the toroidal-field strength in units of the polar value $B_p = 10^{15}$ G. The labels on top of each panel show the toroidal-field energy content $E_{\rm tor}/E_{\rm m}^{\rm int}$. *Bottom panels:* The same as above but with a colour-coded representation of the azimuthal electric current J_ϕ in units of 10^{-5} km^{-1}.

(as done in Papers I and II) but a polytropic choice is sufficient for our purposes and has the advantage that the configurations obtained can be easily employed as initial data for dynamical simulations. Magnetic fields can be considered as a perturbation on the stellar structure as long as the magnetic energy is much smaller than the binding energy and essentially if $\lesssim 10^{17}$ G, see Giacomazzo et al. (2011) for a recent example. In practice, we fix the field strength at the pole to $B_p = 10^{15}$ G, consistent with the observed order-of-magnitude of magnetars.

An equilibrium magnetic-field configuration is found by solving the Grad-Shafranov equation for the unknown function represented by the azimuthal component of the vector potential $A_\phi \equiv \psi(r, \theta)$ (see Paper I and II for details)

$$-\frac{e^{-\lambda}}{4\pi}\left[\partial_r^2\psi + \frac{\partial_r\nu - \partial_r\lambda}{2}\partial_r\psi\right] - \frac{1}{4\pi r^2}\left[\partial_\theta^2\psi - \cot\theta\,\partial_\theta\psi\right]$$
$$= \bar{J}_\phi + F(\rho + 2p)r^2\sin^2\theta$$
$$= \frac{e^{-\nu}}{4\pi}\beta\frac{d\beta}{d\psi} + F(\rho + 2p)r^2\sin^2\theta\,, \quad (1)$$

where the rest-mass density ρ, the pressure p and the metric functions $\nu(r)$, $\lambda(r)$ are known from the background solution, while $\beta(\psi)$ and $F(\psi)$ are two arbitrary functions, the former one expressing the azimutal current $\bar{J}_\phi$. Once a solution is found for ψ, the magnetic-field components can be computed from the curl of the vector potential. As surface boundary conditions we impose that ψ and its derivatives match the exterior vacuum solution. We simplify the problem by assuming that the magnetic field is dipolar and thus that $\psi(r, \theta) = -a_1(r)\sin^2\theta$.

The choice of the trial functions $\beta(\psi)$ and $F(\psi)$ represents a prescription for the current distribution and determines the fi-

nal magnetic field geometry. We recall that the function $\beta(\psi)$ is related to the ratio of toroidal and poloidal fields (i.e., $\beta = 0$ gives a purely poloidal field) and we take one of the simplest forms for a twisted-torus geometry with continuous fields, $\beta(\psi) = \zeta_0 \psi (|\psi/\bar{\psi}| - 1) \Theta(|\psi/\bar{\psi}| - 1)$, where ζ_0 is a constant, $\bar{\psi}$ is the value of ψ on the last closed-field line (the one tangent to the surface) and $\Theta(x)$ is the Heaviside step function, which confines the toroidal field in the closed-line region. Once the second arbitrary function $F(\psi)$ is also chosen, we can vary the constant ζ_0 to obtain a set of configurations with varying toroidal-field content. The simplest and common choice for F is that it is a constant, i.e.,

$$F(\psi) = c_0 \,, \qquad (2)$$

which then leads to the configurations shown in Fig. 1. The initial solution has $\zeta_0 = 0$ (i.e., no toroidal field; left panels) and we increase ζ_0 to reach a higher internal toroidal-to-total magnetic-field energy ratio $E_{\rm tor}/E_{\rm m}^{\rm int}$. As a result, the toroidal field becomes stronger, but the closed-line region also shrinks, so that the amount of toroidal magnetic energy reaches a maximum with $E_{\rm tor}/E_{\rm m}^{\rm int} = 5.5\,\%$ (middle panels) and then starts decreasing (right panels). This happens because the stronger toroidal fields require a stronger electric current in the closed-line region (Fig. 1, bottom panels) and this affects the poloidal field lines by moving the neutral point outwards. In practice, these examples summarize the limitations of the previous twisted-torus models, which could lead to NSs with only $E_{\rm tor}/E_{\rm m}^{\rm int} \lesssim 10\%$. In what follows we discuss how we can overcome these restrictions with a more ingenious choice for $F(\psi)$. For simplicity, we maintain the same form for $\beta(\psi)$ as different choices yield similar results (see Paper II).

The first element of our prescription to increase the amount of toroidal-field energy in the star consists in having a larger region of closed field lines. In absence of toroidal fields, the closed-line region can be enlarged by changing the prescription for $F(\psi)$ so that the electric currents are more concentrated near the symmetry axis. Note that this also implies an increase of the magnetic energy in the star for a fixed external field strength. Pushing this idea to the limit would give a poloidal field entirely confined in the star (see also Fujisawa et al. 2012). If toroidal fields are included, a larger closed-line region would still undergo a contraction, but we expect the maximum toroidal-field energy to be considerably larger. To produce a larger region of closed field lines we extend (2) as

$$F(\psi) = c_0 \left[(1 - |\psi/\bar{\psi}|)^4 \Theta(1 - |\psi/\bar{\psi}|) - \bar{k} \right] \,, \qquad (3)$$

with c_0 and $\bar{k}$ constants.

The second element of our prescription aims instead at reducing the effect that toroidal fields have on poloidal field lines by modifying (3) as $F(\psi) \rightarrow F(\psi) + \bar{F}(\psi)$, with the new term $\bar{F}(\psi)$ chosen so as to cancel as much as possible the toroidal-field contribution to the Grad-Shafranov equation, i.e., the β term in Eq. (1). In practice, we set $\bar{F} = X(\psi)\, \beta\, (d\beta/d\psi)$, so that the complete azimuthal current that we want to minimize is

$$\hat{J}_\phi \equiv \bar{J}_\phi + \bar{F}(\rho + 2p)r^2 \sin^2\theta$$
$$= \beta \frac{d\beta}{d\psi} \left[\frac{e^{-\nu}}{4\pi} + X(\psi)(\rho + 2p)r^2 \sin^2\theta \right] \,. \qquad (4)$$

Making this quantity negligibly small would allow us to add an arbitrarily large toroidal field without changing the closed-line region and thus resulting in an arbitrarily high $E_{\rm tor}/E_{\rm m}^{\rm int}$. Despite our freedom in choosing $X(\psi)$, a perfect cancellation would be possible only in the limit of a magnetic field entirely confined inside the star. Nevertheless, the minimization of $\hat{J}_\phi$ becomes more effective as the closed-line region extends towards the symmetry
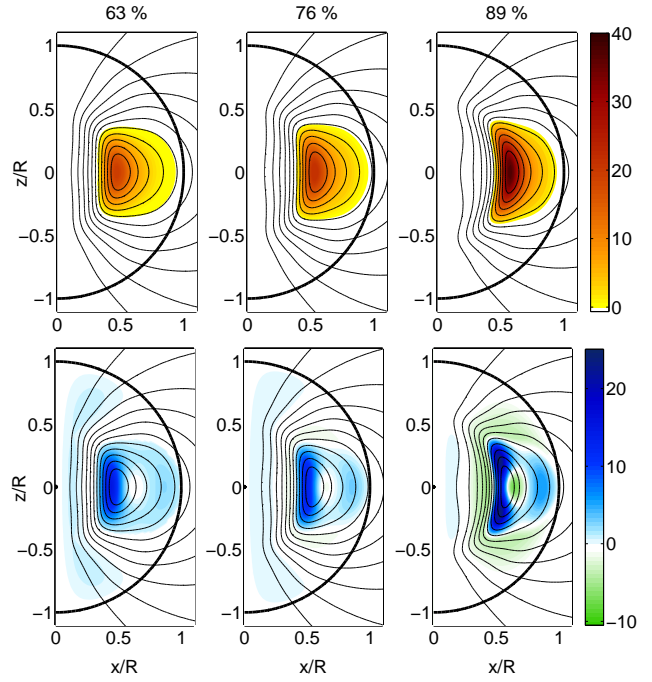

Figure 2. The same as in Fig. 1 for three configurations of maximal $E_{\rm tor}/E_{\rm m}^{\rm int}$ obtained with the new prescription; from left to right $\bar{k} = 0.03, 0.15, 0.35$.

axis and at some point it starts increasing significantly the maximum toroidal-field energy. Again, the possibility of storing more energy in toroidal fields also leads to the increase of the total magnetic energy in the star. Here we simply set $X(\psi) = X_0 = {\rm const.}$, with X_0 fixed so as to minimize $\hat{J}_\phi$. Remarkably, prescription (3) and the addition of $\bar{F}$ have a limited effect if adopted separately, but their combined use yields a significant difference.

3 NEW TWISTED-TORUS SOLUTIONS

Using our new approach we consider different example models with $\bar{k}$ in the range $[0.03, 0.35]$. For each $\bar{k}$, we span the full range of ζ_0, obtaining geometries with varying $E_{\rm tor}/E_{\rm m}^{\rm int}$. All the other constants are fixed once we choose $B_p = 10^{15}$ G. Using the same conventions as in Fig. 1, we show in Fig. 2 the configurations having the maximum toroidal field content for three choices of $\bar{k}$, noting that in general a higher $\bar{k}$ gives a higher energy ratio, up to $E_{\rm tor}/E_{\rm m}^{\rm int} = 89\%$. This extreme case corresponds to a toroidal-field-dominated geometry and clearly demonstrates that the new prescription allows us to overcome the limitations of previous twisted-torus models. Note also from the different colour scale that the new configurations have much stronger maximum toroidal fields $B_{\rm tor}^{\rm max}$, up to $\sim 10^{16}$ G, while the currents are comparable.

Figure 3 provides a more quantitative measure of the magnetic field and the vector potential via the function $a_1(r)$, with the left panel illustrating configurations obtained with $\bar{k} = 0.25$ and increasing $E_{\rm tor}/E_{\rm m}^{\rm int}$, from 40% to 80% (the top part shows the radial profile of the toroidal magnetic field on the equatorial plane, while the bottom part shows the radial profile of $a_1(r)$ for the same models). Note that for fixed $\bar{k}$, a higher toroidal-field content reduces the extension of the closed-line region. On the other hand, as this region expands when keeping fixed the polar field strength B_p, both the interior poloidal and toroidal-field strengths
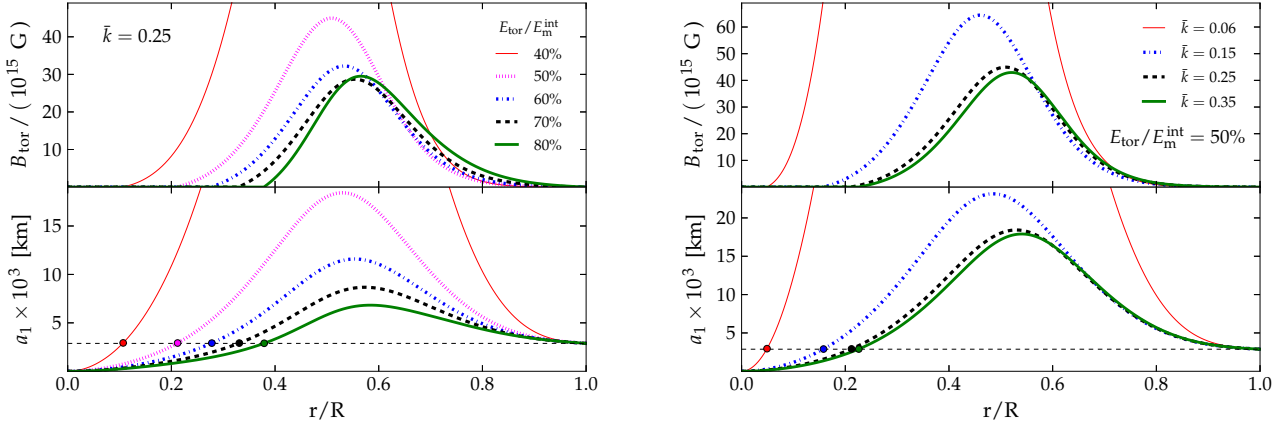
Figure 3. *Left panel:* The top part shows the radial profile of the toroidal magnetic field on the equatorial plane for models with $\bar{k} = 0.25$ and different toroidal-field content $E_{\rm tor}/E_{\rm m}^{\rm int}$. The bottom part, instead, shows the radial profile of $a_1(r) = -\psi(r, \theta = \pi/2)$ for the same models, with the filled dots marking the extension of the closed-line region. *Right panel:* The same as in the left panel, but for models with fixed $E_{\rm tor}/E_{\rm m}^{\rm int}$ and varying $\bar{k}$.

increase very rapidly. In the right panel of Fig. 3 we report the same quantities as in the left one but when varying $\bar{k}$ and imposing $E_{\rm tor}/E_{\rm m}^{\rm int} = 50\%$, i.e., the energy equipartition between poloidal and toroidal fields. As the sequence shows, when approaching $\bar{k} = 0.35$, the strength of the two components rapidly converges to a minimum value. In terms of the internal magnetic energy, this lower limit gives $E_{\rm m}^{\rm int}/E^* \gtrsim 68$, where $E^* \simeq 2.7 \times 10^{48}$ erg is the internal magnetic energy of the purely poloidal model shown in the first panel of Fig. 1. We conclude that for $E_{\rm tor}/E_{\rm m}^{\rm int} = 50\%$, the internal magnetic energy is at least 1-2 orders of magnitude larger than for the poloidal-field-dominated models built with the previous prescription (2) and the same B_p. This result provides an effective example of how a higher toroidal field content implies a much higher internal magnetic energy.

Although our findings depend quantitatively on the particular choice for $F(\psi)$ and $\beta(\psi)$, they imply the following result that we expect to be general for twisted-torus geometries: if a more substantial part of magnetic energy is in the toroidal-field component, i.e., if $E_{\rm tor}/E_{\rm m}^{\rm int} \gtrsim 10\%$, then higher internal magnetic energies are not only possible but rather inevitable.

4 QUADRUPOLAR DEFORMATIONS

Magnetic fields alter the NS density and pressure distributions inducing quadrupolar deformations that can be quantified in terms of the quadrupolar ellipticity $\epsilon_Q \equiv Q/I$, where Q is the mass-energy quadrupole moment and scales as the magnetic energy (i.e., $\propto B^2$), while I is the mean value of the stellar moment of inertia [see also the discussion by Frieben & Rezzolla (2012) on the difference between surface and quadrupolar ellipticities]. Poloidal fields deform a nonrotating star towards an oblate shape (equatorial radius larger than the polar radius), corresponding to positive ϵ_Q, whereas toroidal fields have the opposite effect; therefore, the amount of deformation is reflected in the toroidal-to-poloidal energy ratio. In general, a magnetized NS that rotates around an axis misaligned with respect to the magnetic axis and having $\epsilon_Q \neq 0$, will emit a continuous GW signal with amplitude $h \propto |\epsilon_Q| I \Omega^2/d$ (Bonazzola & Gourgoulhon 1996), where Ω is the angular velocity and d the source distance from the observer. Following the procedure adopted in Paper II, we can compute the deformations of

our new set of configurations and compare them with the typical predictions of previous twisted-torus models. Considering a set of realistic EOSs would introduce a variance of ~ 2 in the results (see Paper II); however, here we are concerned with the influence that the magnetic field geometry has on the deformation, which is independent of the particular EOS adopted.

In Table 1 we report the results for some representative solutions, with the first two lines referring to configurations obtained with prescription (2), corresponding to the purely poloidal model and to one with maximal toroidal energy (first two columns in Fig. 1). These models are representative of the order-of-magnitude deformations obtained with the poloidal-field-dominated solutions proposed so far in the literature. The other lines refer to our new configurations with different values of $\bar{k}$ and toroidal magnetic energies. In addition to ϵ_Q for $B_p = 10^{15}$ G, we also show its value normalized to the internal magnetic energy $E_{\rm m}^{\rm int}$ (expressed in km). This quantity is independent of the magnetic-field strength and only depends on the geometrical distribution.

As mentioned above, the sign of ϵ_Q results from the balance between poloidal (positive) and toroidal (negative) field deformations and the separation occurs around equipartition, i.e., $E_{\rm tor}/E_{\rm m}^{\rm int} \sim 50\%$, indicating that such balance is essentially controlled by the amount of energy in the two components. The same can be deduced by looking at the normalized ellipticities $\epsilon_Q/E_{\rm m}^{\rm int}$. These are smaller when $E_{\rm tor}/E_{\rm m}^{\rm int} \simeq 40 - 50\%$, where the two kind of deformations are well balanced, and they grow when moving away from equipartition. In particular, similar (and opposite) values are found in the poloidal-field-dominated and in the toroidal-field-dominated case. Note that different values of $\bar{k}$ with the same toroidal energy content give only slightly different $\epsilon_Q/E_{\rm m}^{\rm int}$. Most importantly, the majority of the new configurations considered has $|\epsilon_Q| \sim 10^{-4} \times (B_p/10^{15} \text{ G})^2$, which is at least *one order of magnitude* larger than the values given by poloidal-field-dominated geometries. This is due to the much higher internal magnetic energies obtained for geometries with higher $E_{\rm tor}/E_{\rm m}^{\rm int}$. In summary, twisted-torus configurations with higher toroidal energy content, say, $E_{\rm tor}/E_{\rm m}^{\rm int} \geqslant 40\%$, can easily produce GW amplitudes that are one order of magnitude larger than what predicted so far, either in newly-born magnetars or in pulsars with large buried fields, with an obvious enhancement of their detectability. Moreover, in magnetized NSs with negative ellipticities, a spin-flip

$\bar{k}$	$E_{\rm tor}/E_{\rm m}^{\rm int}$	ϵ_Q	$\epsilon_Q/E_{\rm m}^{\rm int}$ [km^{-1}]	$B_{\rm tor}^{\rm max}/B_p$
–	0.0 %	$+9.8 \times 10^{-6}$	$+4.43$	0
–	5.5 %	$+5.1 \times 10^{-6}$	$+3.59$	2
0.03	63 %	-2.7×10^{-5}	-1.54	20
0.06	50 %	-5.5×10^{-3}	-0.47	549
0.06	67 %	-3.6×10^{-5}	-1.90	20
0.15	50 %	-1.5×10^{-4}	-0.55	64
0.15	76 %	-5.6×10^{-5}	-2.75	22
0.25	40 %	$+1.0 \times 10^{-4}$	$+0.06$	142
0.25	50 %	-1.0×10^{-4}	-0.65	45
0.25	60 %	-1.0×10^{-4}	-1.37	32
0.25	70 %	-1.1×10^{-4}	-2.14	29
0.25	80 %	-1.4×10^{-4}	-2.99	30
0.25	84 %	-1.2×10^{-4}	-3.40	30
0.35	50 %	-1.0×10^{-4}	-0.70	43
0.35	89 %	-1.9×10^{-4}	-3.74	38

Table 1. Summary of the properties of models built with prescription (2) (first two lines) and with the new prescription (3), for $B_p = 10^{15}$ G.

mechanism driven by viscosity may occur, leading to an increase in the angle between the spin and magnetic axes, which tend to become nearly orthogonal (Jones 1975; Cutler 2002). In this case, the GW emission would be further enhanced, with optimistic prospects of detection (Stella et al. 2005).

5 CONCLUDING REMARKS

We have discussed a novel procedure for obtaining twisted-torus equilibrium configurations of nonrotating magnetized NSs where the magnetic field energy in the toroidal component can be as high as the poloidal one, or even higher. In previous twisted-torus models based on a simpler prescription for the electric currents, in fact, the toroidal magnetic energy was at most $\sim 10\%$ of the total. However, with a suitable choice of the azimuthal currents it is possible to build new equilibria with toroidal fields containing up to $\sim 90\%$ of the total internal magnetic energy and toroidal magnetic fields that are on average about three times larger than the poloidal ones. When compared with the poloidal-field-dominated geometries proposed in the past, our configurations represent equally valid candidates for NS interiors and possibly more realistic ones.

An important implication of our findings is that for a fixed exterior field strength, stars with larger energy in toroidal-fields have to have a much larger magnetic energy stored in the interior. As a result, if NSs have internal magnetic fields close to a twisted-torus geometry with a high toroidal content, say, $E_{\rm tor}/E_{\rm m}^{\rm int} \gtrsim 10\%$, then the internal magnetic energy would be higher than commonly assumed, with a potentially strong impact on the emission properties. As an example, for the new solutions with $E_{\rm tor}/E_{\rm m}^{\rm int} \gtrsim 40\%$, the GW emission associated with the magnetically induced stellar deformations is about one order of magnitude larger than for poloidal-field-dominated configurations.

Finally, the new toroidal-field-dominated configurations could be stable over several Alfvén timescales, in contrast with what known for poloidal-field-dominated stars. Should this be confirmed by nonlinear simulations, it would provide strong support to the idea that these configurations are realistic representations of the stellar interior. This will be considered in our future work.

REFERENCES

Bonanno A., Rezzolla L., Urpin V., 2003, A&A, 410, L33
Bonazzola S., Gourgoulhon E., 1996, A&A, 312, 675
Braithwaite J., 2009, MNRAS, 397, 763
Braithwaite J., Nordlund Å., 2006, A&A, 450, 1077
Chandrasekhar S., Fermi E., 1953, ApJ, 118, 116
Ciolfi R., Ferrari V., Gualtieri L., 2010, MNRAS, 406, 2540
Ciolfi R., Ferrari V., Gualtieri L., Pons J. A., 2009, MNRAS, 397, 913
Ciolfi R., Lander S. K., Manca G. M., Rezzolla L., 2011, ApJ, 736, L6
Ciolfi R., Rezzolla L., 2012, ApJ, 760, 1
Colaiuda A., Ferrari V., Gualtieri L., Pons J. A., 2008, MNRAS, 385, 2080
Cutler C., 2002, PRD, 66, 084025
Duez V., Mathis S., 2010, A&A, 517, A58
Duncan R. C., Thompson C., 1992, ApJ, 392, L9
Frieben J., Rezzolla L., 2012, MNRAS, 427, 3406
Fujisawa K., Eriguchi Y., 2013, MNRAS, 432, 1245
Fujisawa K., Yoshida S., Eriguchi Y., 2012, MNRAS, 422, 434
Giacomazzo B., Rezzolla L., Baiotti L., 2011, PRD, 83, 044014
Glampedakis K., Andersson N., Lander S. K., 2012, MNRAS, 420, 1263
Haskell B., Samuelsson L., Glampedakis K., Andersson N., 2008, MNRAS, 385, 531
Ioka K., Sasaki M., 2004, ApJ, 600, 296
Jones P. B., 1975, Astrophysics and Space Science, 33, 215
Kiuchi K., Yoshida S., Shibata M., 2011, A&A, 532, A30
Lander S. K., 2013, PRL, 110, 071101
Lander S. K., Jones D. I., 2009, MNRAS, 395, 2162
Lander S. K., Jones D. I., 2012, MNRAS, 424, 482
Lasky P. D., Zink B., Kokkotas K. D., 2012, ArXiv e-prints, arXiv:1203.3590
Lasky P. D., Zink B., Kokkotas K. D., Glampedakis K., 2011, ApJ, 735, L20
Markey P., Tayler R. J., 1973, MNRAS, 163, 77
Pons J. A., Perna R., 2011, ApJ, 741, 123
Stella L., Dall'Osso S., Israel G. L., Vecchio A., 2005, ApJ, 634, L165
Tayler R. J., 1973, MNRAS, 161, 365
Thompson C., Duncan R. C., 1993, ApJ, 408, 194
Tomimura Y., Eriguchi Y., 2005, MNRAS, 359, 1117
Wright G. A. E., 1973, MNRAS, 162, 339
Yoshida S., Eriguchi Y., 2006, ApJ Suppl., 164, 156
Yoshida S., Kiuchi K., Shibata M., 2012, PRD, 86, 044012
Zink B., Lasky P. D., Kokkotas K. D., 2012, PRD, 85, 024030